RSC Advances

ROYAL SOCIETY
OF CHEMISTRY

www.rsc.org/advances

Journal Name

ARTICLE

Triple helical collagen-like peptide interactions with selected polyphenolic compounds

M. E. Plonska-Brzezinska*[a], D. M. Bobrowska[a], A. Sharma[b], P. Rodziewicz[a], M. Tomczyk[c], J. Czyrko[a] and K. Brzezinski*[a]

Because collagen is the most abundant component of connective tissue, it is an excellent biomaterial in numerous medical applications. However, the utility of collagen is limited by its low mechanical strength in aqueous solutions and its susceptibility to proteolytic degradation *in vivo*. To improve the physical properties of collagen and to enhance its chemical resistance, it is necessary to stabilize its structure through chemical or physical modifications. In this study, we analyzed the interactions of a model molecule, a synthetic triple helical collagen-like peptide, with polyphenols such as curcumin, rutin, quercetin, naringin, and hypericin. Interactions between the peptide and polyphenolic compounds were analyzed using various techniques. The layer-by-layer assembly processes of a gold surface using the peptide and polyphenols was performed via surface plasmon resonance (SPR), atomic force microscopy (AFM), and ellipsometry. SPR screening of polyphenols was conducted in real time to select compounds that bind to the collagen-like peptide and could thus be applied to the stabilization of collagen. Selected polyphenols, especially naringin and hypericin, demonstrated notable binding to the peptide. To determine the nature of these interactions, experiments were supplemented with crystallographic studies and molecular docking of plant metabolites and collagen-like peptides.

Introduction

Nanotechnology is the creation and control of the properties of nanometric-scale objects. Nanotechnology plays an increasingly significant role in medicine, material engineering, and pharmacology. The interaction of small molecules with proteins plays an important role in the regulation of biological processes. The identification and study of these interactions are crucial in the understanding of many biological processes and the design of new pharmaceuticals.

Why is collagen the subject of our interest? Collagen is important due to its various mechanical properties, such as tensile strength, stability, and elasticity,[1,2,3] and is therefore the most important structural protein in extracellular matrices and connective tissues in animals, especially in skin, bones, cartilage, and basement membranes.[4] Collagen is also the primary component of the cardiovascular system.[5,6] Due to its non-immunogenicity, excellent biocompatibility and biodegradability, collagen has been widely used as a biomaterial in the pharmaceutical and medical fields[7,8,9] and as a carrier for drug delivery.[10]

The unique biological and structural properties of collagen are due to its structure. The collagen molecule is typically composed of a very long triple helix with a specific and repeating glycine-proline-hydroxyproline or glycine-X-hydroxyproline pattern, where X corresponds to other natural amino acids. The structure of the triple helix is stabilized by interchain hydrogen bonds.[11,12,13] At a higher level of organization, collagen molecules are arranged into fibrils of great strength and stability.[14]

Various approaches have been used to incorporate collagen into artificial constructs for the replacement and regeneration of damaged tissues. Implanted collagen is quickly degraded in aqueous solutions and in the presence of proteolytic enzymes; a stabilization procedure is thus required in this scenario.[15,16,17,18] This stabilization is typically performed via cross-linking approaches.[19,20,21,22,23] Glutaraldehyde has been extensively studied and is often associated with increased tissue mineralization.[24,25] Alternative reagents that are less toxic or that give nontoxic degradation products include formaldehyde, glyceraldehyde, genipin, diisocyanates, proanthocyanidins, chitosan, and 1-ethyl-3-(3-dimethylaminopropyl)carbodiimide.[27,27,28,29] Polyphenolic compounds also bind to collagen and stabilize its resistance to enzymatic degradation.[30,31,32] The interactions between collagen and polyphenols could occur through (i) hydrogen bonds, (ii) hydrophobic associations between the aromatic rings of polyphenols and the pyrrolidine rings of protein, and (iii) polar interactions.[33,34]

Polyphenolic compounds exert protective effects on human health and have been applied in the prevention of cardiovascular diseases.[35,36,37] Polyphenols are a large group of natural compounds that are widely distributed as secondary metabolites in the plant kingdom.[38] These compounds perform a wide spectrum of biological and pharmacological activities. Polyphenols exhibit antioxidant,[39] anti-inflammatory,

a. Institute of Chemistry, Faculty of Chemistry and Biology, University of Bialystok, Hurtowa 1, 15-399 Bialystok, Poland. E-mails: mplonska@uwb.edu.pl, k.brzezinski@uwb.edu.pl.
b. Laboratoire de Chimie Moléculaire, Ecole Polytechnique, CNRS, 91128 Palaiseau Cedex, France
c. Department of Pharmacognosy, Faculty of Pharmacy, Medical University of Bialystok, Mickiewicza 2a, 15-230 Bialystok, Poland.

antimicrobial, and anticarcinogenic activities.[40,41] Additionally, the hepato- and nephroprotective, thrombosis-suppressing, hypoglycemic, and antirheumatic effects of these compounds are well established.[42,43,44,45]

There are two types of biosensors, which differ in regard to their mode of signal generation. For direct bioaffinity sensors, a binding of the analyte results in a change in the conformation of the biomolecule and/or physical changes, such as those associated with charge, thickness, temperature or optical parameters.[46,47] The assembly of proteins on the surface can be performed via several methods, such as polymer or sol-gel entrapment,[48,49] covalent attachment,[50] or physical adsorption.[51]

Optical sensors are important tools given their high sensitivity. Optical surface plasmon resonance (SPR) spectroscopy is used in the *in situ* real-time characterization of solid/liquid interfaces.[52] Its rapidity, high selectivity and sensitivity as well as a label-free procedure have encouraged the wide use of SPR spectroscopy in the study of the interactions of macromolecules with ligands.[53,54] The interaction of a molecule immobilized on the SPR chip surface with its counterpart in solution is monitored using interfacial refractive index changes associated with affinity binding interactions. SPR signals depend on the electron density, effective mass, particle shape, size, dielectric properties and the associated environment.[58,56]

Herein, we analyzed and compared the interactions of some polyphenolic compounds with a triple helical collagen-like peptide [(Pro-Hyp-Gly)$_4$-Pro-Hyp-Ala-(Pro-Hyp-Gly)$_5$]$_3$, which serves as a model molecule for a natural collagen protein. Understanding the nature of interactions between the peptide and polyphenols requires the combination of a broad spectrum of experimental and theoretical methods, such as those applied within these studies. We applied SPR spectroscopy to obtain information on the interactions of a triple-helical collagen-like peptide selected with polyphenolic compounds. Additionally, atomic force microscopy (AFM), ellipsometry, crystallography and molecular docking simulations were performed because they represent excellent tools for the elucidation of the structural and molecular properties of various materials and their peptide-ligand interactions.[57,58]

Results and Discussion

Covalent Functionalization of SPR Slide with the Collagen-like Peptide

To effectively monitor of polyphenolic compound interactions with collagen, it was crucial to prepare a biosensor surface. Self-assembled monolayers (SAM) represents one procedure for biomolecule immobilization.[59,60] The fabrication of a Au disk on a glass substrate was based on the utilization of thiol-ended molecules, which provide extensive and stable bond formation with the surface (Scheme 1).
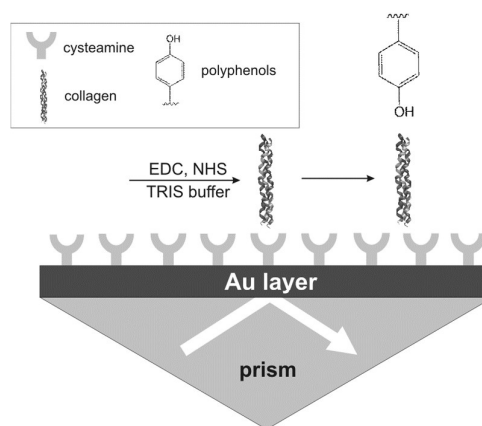
Scheme 1. Scheme of layer-by-layer modification of a Au surface. Abbreviations: EDC: 1-(3-dimethylaminopropyl)-3-ethylcarbodiimide hydrochloride; NHS: N-hydroxysuccinimide.

quercetin (1)

rutin (2)

naringin (3)

hypericin (4)

enol form

keto form

curcumin (5)
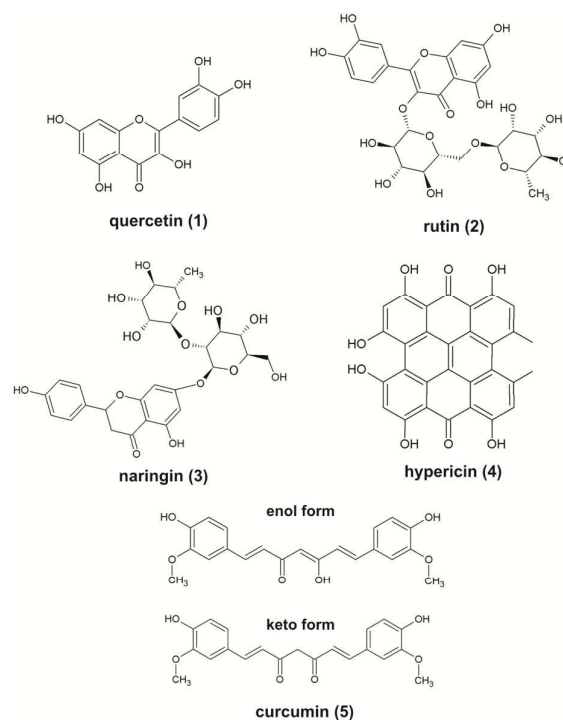
Prior to measurement, an SPR disk was immersed in anhydrous ethanol and was carefully sonicated to remove impurities. After pre-treatment, a Au surface was directly modified with cysteamine to create specific sites for covalent attachment of the collagen-like peptide (Scheme 1). All samples were prepared in 10 mM Tris-buffered saline, pH 8.0. First, 20 mM cysteamine solution was applied to the Au surface for 2 h. The cysteamine layer forced the covalent attachment of collagen to the amine-terminated thiolate layer. Then, the disk was thoroughly rinsed with ethanol and distilled water. After drying under nitrogen, the cysteamine-modified slide was exposed to a collagen solution (20 μL, 10^{-4} mg mL^{-1}) for 1 h. For this procedure, collagen was dissolved in 10% acetic acid to a final concentration of 0.1 mg mL^{-1}. After overnight

incubation at 4°C, acetic acid was replaced with Tris-buffered saline, pH 8.0. The peptide was activated by the carbodiimide, 1-(3-dimethylaminopropyl)-3-ethylcarbodiimide hydrochloride (EDC, 40 μL, 100 mg mL^{-1}) and N-hydroxysuccinimide (NHS, 40 μL, 50 mg mL^{-1}), which were dissolved in 100 μL of the buffer. The resulting product enabled covalent coupling to the Au disk surface. The thiol/peptide-modified Au surface was exposed to solutions containing the five different polyphenols: quercetin (**1**), rutin (**2**), naringin (**3**), hypericin (**4**) and curcumin (**5**). The SPR disk is a flow cell through which an aqueous solution with an appropriate polyphenols was passed continuously. The modifications were prepared using the same procedure and concentration of polyphenols (2×10^{-2} mg mL^{-1}); only the different polyphenolic compounds were applied (50 μL solution of each polyphenol).

Structure of the Collagen-like Peptide
Investigations of numerous polypeptide sequences have demonstrated that inter- and intra-molecular interactions play key roles in forming assemblies and fibrillar structures. For instance, the fibrillar structure of protein may be utilized as a scaffold for ligand interactions, such as tissue grafts in medical applications, an enzymatic linear substrate for the creation of magnetic or conductive nanowires, oriented liquid crystalline components, or gel-forming components.

Collagen-like peptides typically crystallize at an acidic pH in the presence of acetic acid or acetic buffer.[13,61,62] Within this study, the peptide was crystallized in a solution containing 5% acetic acid. A low pH value ensures that the peptide adopts a triple helical form in solution.[63,64] However, polyphenols (and especially their glycosides) are not stable at acidic solutions. Additionally, their solubility is lower. Therefore, to reconcile the need for a low pH value for the proper oligomeric state of the peptide with the low solubility and instability of the ligands solutions, the obtained crystals were transferred to a basic solution (pH=8.0) prior to soaking with polyphenolic compounds. Despite a dramatic change in the pH value, the crystals did not suffer during the soaking experiment. Afterwards, polyphenols were added in a suspension. A suspension was used given the low solubility of the ligands even at higher pH values.

Diffraction data were collected for the four crystals, which were soaked with curcumin, rutin, quercetin or naringin. The highest resolution data correspond to the crystal soaked with quercetin (1.27 Å). None of the ligands were identified in electron density maps, clearly indicating unsuccessful soaking of the peptide crystals with the ligands. Therefore, is the subsequent studies are based on a structure derived from crystals soaked with quercetin (PDB code 4Z1R; this work). The lack of bounded ligands can be explained as a result of low ligand solubility, a lack of ligand binding cavity and/or tight crystal packing. The success of the soaking experiment strongly depends on ligand concentration. As a rule of thumb, ligand molarity is at least ten-fold higher than its target protein. In our experiment, the peptide concentration was 1.2 mM (for the triple helical form). Thus, the concentration of polyphenolic compounds in soaking buffer should be approximately 12 mM

or greater. Moreover, there is no well-established ligand binding site in the structure, and the only possible interactions can occur on the surface of the triple helix. Therefore, we postulate that the ligand concentrations were too low to obtain peptide-polyphenol complexes in the crystal due to low solubility. Another issue involves tight crystal packing of the collagen-like peptide, which can be an obstacle to a ligand's diffusion through the crystal lattice. On the one hand, channels accessible to a solvent are present along planes perpendicular to the x direction and are formed by N- and C-terminal tails of the peptide (Fig. 1a). On the other hand, parallel triple helices are tightly packed and can therefore significantly limit ligand diffusion (Fig. 1b). However, notably, the solvent structure near triple helices changes when crystals are incubated in a solution containing Tris-buffered saline (pH 8.0) and 20% PEG 400. The primary difference is a lack of acetate anions in a crystal lattice after incubation. This observation indicates that the diffusion process is possible at least for solvent molecules within the crystal lattice of the collagen-like peptide.
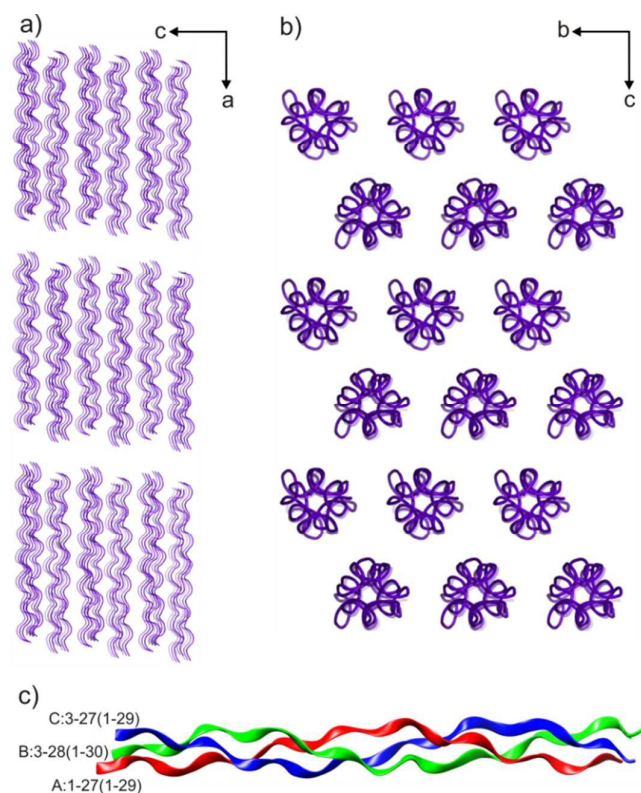

Fig. 1. Packing of the triple helical collagen-like peptide molecules in the current structure (a, b). (a) The structures are projected along the *yz* plane. (b) The structures are projected down the crystal *a*-axis. (c) The molecular structure of the (Pro-Hyp-Gly)$_4$-Pro-Hyp-Ala-(Pro-Hyp-Gly)$_5$ trimer. Chains A, B and C are shown in red, green and blue, respectively; the numbers correspond to the residues included in the 4Z1R and (1CAG) models, respectively.

The structure of collagen-like peptide derived from crystals soaked at the basic pH (PDB code 4Z1R; this work) is very similar to that of the peptide crystalized in the presence of

acetic acid (PDB code 1CAG).[13] The Cα root-mean square deviation between two triple helical peptide models is 0.37 Å for 77 atoms. The main difference between the two compared structures is the disorder observed at the N- and C-terminal tails in the 4Z1R model (Fig. 1c). A change in pH from acidic to basic results in the deprotonation of terminal carboxylic groups. Consequently, negatively charged COO⁻ groups repulse each other and destabilize the C-terminal end of the triple helix. In contrast to the 1CAG model, the current structure N-terminal tail of the triple helix is also disordered. In both crystal structures, the N-terminal proline residue is positively charged; the pKa value for the imino acid ring of the proline residue is approximately 10.6. However, in the 1CAG model, the N-terminal tail is stabilized by interactions with a well-ordered C-terminal tail of the triple helix from an adjacent unit cell. In the 4Z1R model, the C-terminal end is disordered and therefore cannot significantly participate in the stabilization of the opposite end of the neighbouring peptide.

Collagen-like peptide adopts triple helical structure at acidic pH, but AFM and SPR experiments were performed at basic pH

to avoid hydrolysis of polyphenolic compounds. Prior to AFM and SPR, the peptide was dissolved and incubated in acetic acid. Prior to further experiment the acid was replaced by the basic buffer. The question arises if the structure at acidic and basic pH is the same. Presented crystal structure clearly shows that dramatic change in the pH does not affect the molecular structure of the peptide.

Atomic Force Microscopy

Atomic force microscopy (AFM) is a useful tool for monitoring the topography of the surface and for studying the interactions between the AFM tip and the sample. In this study, the interactions between polyphenolic compounds and collagen were assessed using the dynamic AFM mode (tapping mode).
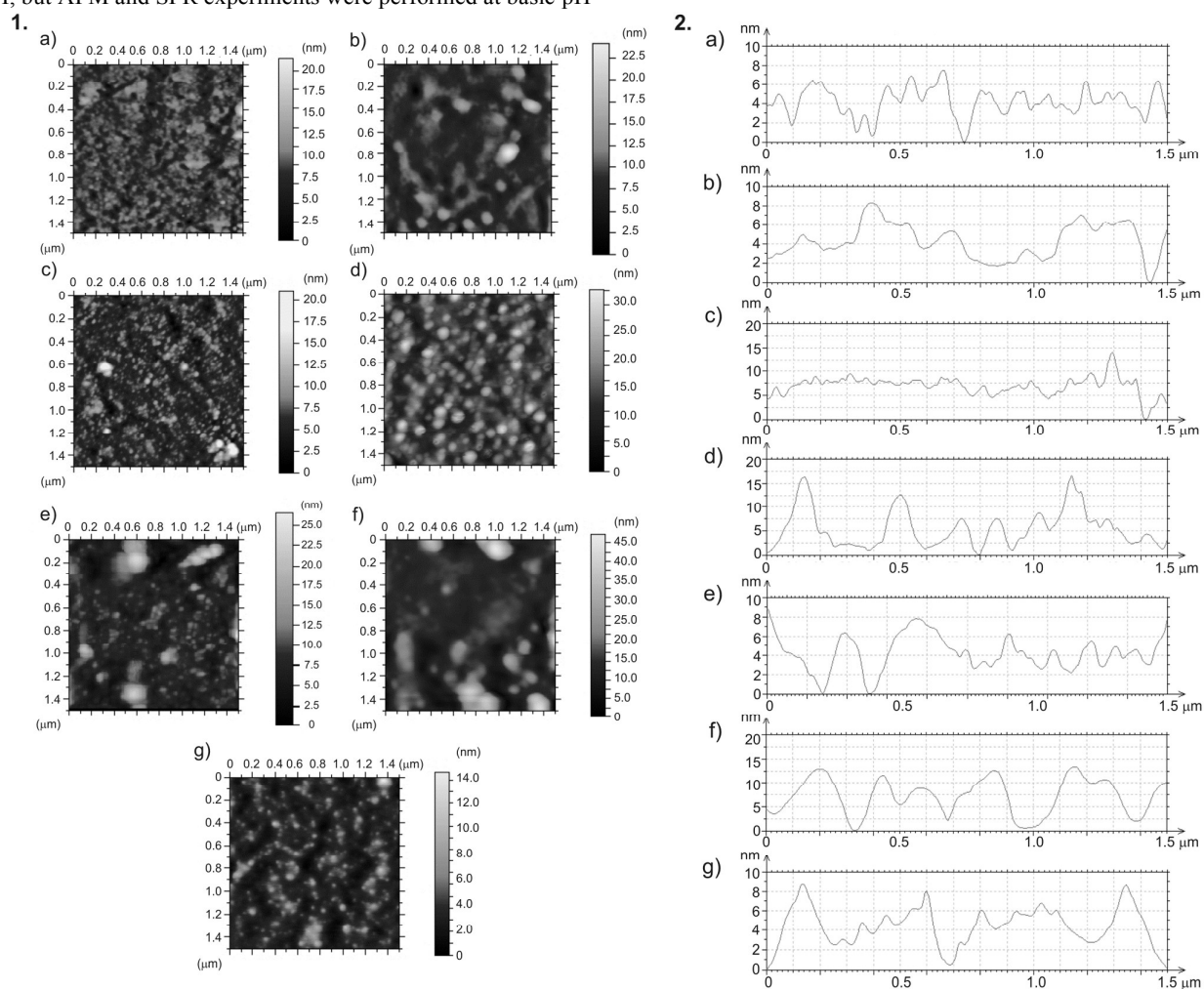

Fig. 2. (1) Tapping mode AFM images of topography and (2) corresponding topographic cross-section analyses of AFM images of a Au surface modified with (a) cysteamine and (b) collagen. The Au/cysteamine/collagen layers were immobilized by polyphenols: (c) curcumin, (d) rutin, (e) quercetin, (f) naringin, and (g) hypericin.
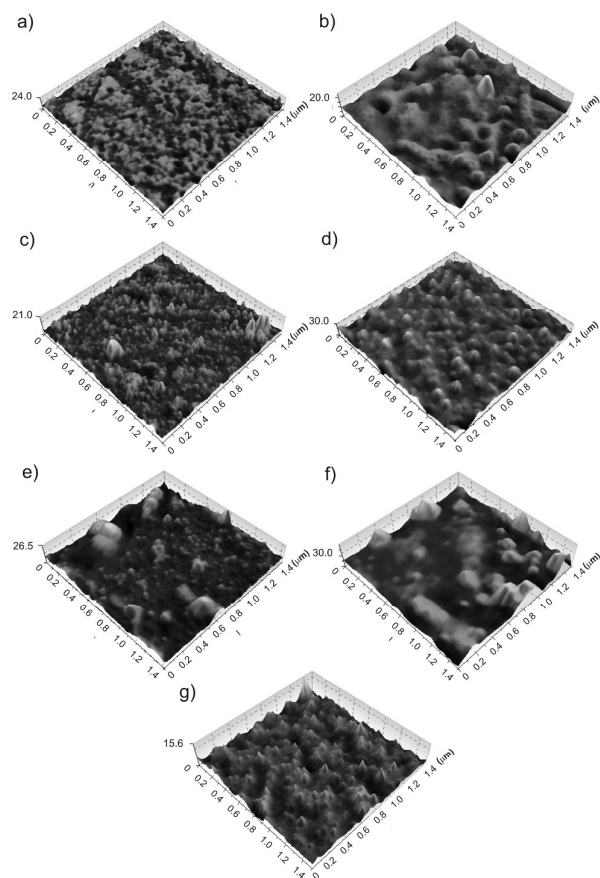
Journal Name

ARTICLE

Fig. 3. Tapping mode AFM images of 3D topography of Au modified with cysteamine (a) and then functionalized collagen (b). On the top of Au/cysteamine/collagen layer was immobilized by polyphenols: curcumin (c), rutin (d), quercetin (e), naringin (f) and hypericin (g).

In the AFM tapping mode, the cantilever oscillates with the probing tip close to its free resonance frequency at a given amplitude.[65] The interaction between the sample and the probe gives rise to surface topographies (height) and morphologies (phase). Surface-sensitive methods, such as AFM, which are commonly used to investigate adsorption processes, require surfaces that are not atomically flat (e.g., Au). The AFM images provide topographic views of thiol, collagen and immobilized polyphenols on the modified Au surface. The presence of each monolayer was reliably detected via force measurements and imaging.

Figures 2 and 3 depict representative two-dimensional (2D) and three-dimensional (3D) reconstructions of 1.5×1.5 μm AFM images

both prior to and after the immobilization of collagen and after chemical treatment with polyphenols. Figures 2a panel(1) and 3a present representative surface topographies from tapping mode AFM images of cysteamine layers adsorbed on a Au SPR surface. Sample preparation was performed in ethanol solution using 20 mM cysteamine for 2 h. Different contrasts for the same molecules suggest that the cysteamine molecules may adsorb on the gold surface in several conformations.[66] We determined the image root mean square (RMS) of formed layers on a Au surface. The image root mean square (a measure of layer roughness) represents the standard deviation of the height values within a given area.[67] The RMS of the Au substrate with chemically adsorbed cysteamine was ca. 1.71 nm.

Next, the Au/cysteamine surface was immersed in 10^{-4} mg mL^{-1} collagen solution in the presence of activators (EDS and NHS), resulting in peptide binding to the cysteamine molecules. Collagen was immobilized on substrate surfaces via a two-step procedure, which was previously described. The peptide formed aggregates with different sizes with diameters ranging from 0.138 to 0.311 μm and heights varying from 1.13 to 4.13 nm (Fig. 2b panels (1) and (2) and Fig. 3b). After collagen attachment, RMS increased to 2.09 nm for a 1.5 x 1.5 μm area, indicating a rougher surface due to the presence of the peptide attached to the thiol layer.

Further, a thiol/the peptide-modified gold surface was subject to the solution of five compounds: curcumin, rutin, quercetin, naringin and hypericin (Figs. 2c-2g and 3c-3g). The domains on the Au/cysteamine/peptide surface were identified for all polyphenols. Qualitative comparisons between the peptide-modified surface and polyphenols revealed non-uniform binding and indicated binding to specific locations across the surface. The Au/cysteamine/peptide surface presented a heterogeneous distribution of polyphenolic compounds. The AFM images demonstrate that the sizes of domains and pits depend on the immobilized compounds. The 2D and 3D topographic images demonstrated (Fig. 2, panel (1) and Fig. 3) that curcumin, rutin and hypericin molecules were thoroughly distributed across the collagen-modified surface. The above-mentioned tapping mode AFM images demonstrate the presence of a uniform high density of small domains. The surfaces coated with curcumin, rutin, and hypericin exhibited average roughness values (RMS) of 1.74, 3.53, and 1.59 for a 1.5 x 1.5 μm area, respectively. After being adsorbed with curcumin and hypericin (Figs. 2c, 3c, 2g, and 3g), the surfaces of the Au/thiol/peptide became more regular and produced relatively thicker and more mounted polyphenolic coatings. Numerous irregularly shaped particles were observed on the Au surface that was coated with quercetin and naringin (Figs. 2e, 2f, 3e and 3f). According to the surface roughness data, the

RMS values increased for quercetin (3.3 nm. Figs. 2e and 3e) and naringin (5.84 nm) for 1.5 x 1.5 μm areas (Figs. 2f and 3f).

These AFM imaging observations support the possible interaction between collagen-like peptides and polyphenolic molecules (**1-5**).

Surface Plasmon Resonance Spectroscopy and Ellipsometry

To further investigate the binding specificity of the polyphenolic compounds to the triple helical collagen-like peptide, SPR was applied. This method is capable of detecting self-assembled monolayers and monitoring interactions on the molecular level. Materials adsorbed on surfaces alter SPR reflectivity and allow the determination of the effective thicknesses of the adsorbed or covalently attached material. In SPR experiments, analytes are passed over the sensor chip through a microfluidics system, and the binding process is monitored in real time.[68] Quantitation is based on the variation of the SPR parameters, such as shifts of the resonance angles (*Surface Plasmon Angle*, $\Delta\theta_{SPR}$) at the reflectance minimum.

The fabrication of SPR slides was performed as described above. After nanodisk fabrication, each step of the SPR angular reflectance curve (*R-θ*) was collected (Fig. 4). All of the spectra were recorded in 10 mM Tris-buffered saline (TRIS, pH 8.0) after thoroughly rinsing the samples to remove the nonspecifically bonded biomolecules (solution TRIS/Tween-20). The experimentally measured shifts of the SPR angles are listed in Table 1. $\Delta\theta_{SPR}$ and $\delta\theta$ refer to the resonance angle between two neighbouring monolayers and the difference of the resonance angles compared with a bare gold SPR, respectively.

Table 1. SPR angle shifts.

Layer	$\delta\theta_{SPR}^{[a]}$ (°)	$\Delta\theta_{SPR}^{[b]}$ (°)
Au	0	0
Cysteamine	0.117	0.117
Collagen-like peptide	0.312	0.195
Curcumin	0.348	0.036
Rutin	0.417	0.105
Quercetin	0.414	0.102
Naringin	0.448	0.136
Hypericin	0.658	0.346

[a] $\delta\theta$ refers to the difference of the resonance angles from a bare gold SPR; [b] $\Delta\theta$ refers to the difference of the resonance angles between the top layer and neighbouring layer.

SPR sensograms revealed different characteristics of binding of the polyphenols (analytes) to the Au/thiol/peptide surface. The refractive index in the vicinity of the surface is altered during the interactions, and the SPR angle is correspondingly shifted (Fig. 4). Subsequent polyphenol injection leads to a typical SPR response, which represents the binding of the polyphenolic molecules on the surface. This signal directly correlates with the amount of polyphenols interacting near the SPR surface with the collagen-like peptide. Fig. 4f shows appropriate control experiments to present that the observed collagen-like peptide binding activity is specific. The spectra were recorded using a Au/cysteamine surface and quercetin (Q) or hypericin (H) as a negative control. Q or H were passed over the sensor chip through a microfluidics system. We did not observed binding process with a Au/cysteamine surface, that

confirmed luck of a specific interaction of the SPR surface (Au/cysteamine) with the polyphenolic molecules.
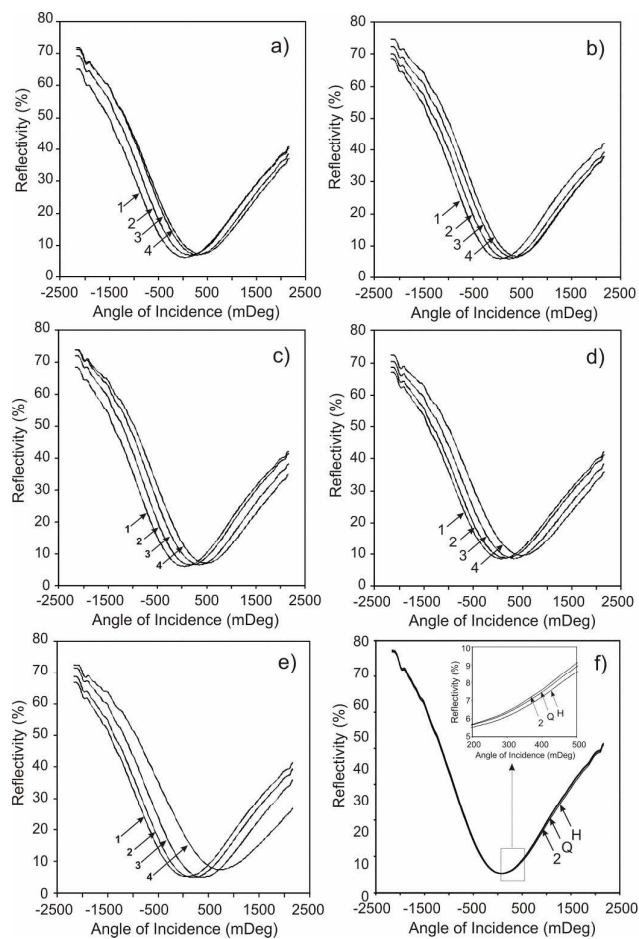
Fig. 4. SPR reflectivity of each step of (1) Au surface modified with (2) cysteamine, (3) collagen and (4) polyphenols: curcumin (a), rutin (b), quercetin (c), naringin (d) and hypericin (e). (f) Control sample: SPR reflectivity of each step of (2) Au surface modified with cysteamine, and quercetin (Q) or hypericin (H).
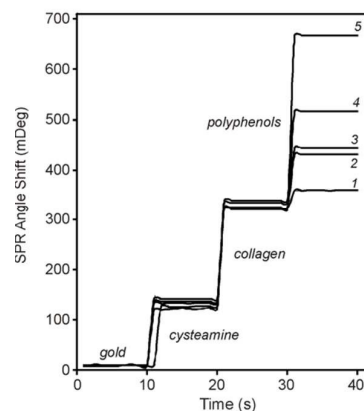

Fig. 5. Sensograms of the assembly of polyphenols into the Au/cysteamine/collagen surface. In each step, different compounds were injected: (1) curcumin, (2) rutin, (3) quercetin, (4) naringin, and (5) hypericin.

To confirm the interaction of analytes with the peptide, we also performed time-based analyses. The results of SPR reflectivity are presented as a sensogram, which is a plot of changes in the resonance signal as a function of time (Fig. 5). The interaction was detected for five polyphenolic compounds at concentrations of approximately 2×10^{-5} M that promoted a linear shift variation. The detailed modification steps presented in Scheme 1 with the corresponding extinction peak shift of SPR sensors are presented in Figure 5.

The greatest affinity was observed for hypericin (Fig. 5). Thus, the order of affinity for the peptide was hypericin>naringin>quercetin>curcumin>rutin. The reason for the differences in the binding patterns can be attributed to the differences in the structures of polyphenols. The hydroxyl groups of polyphenols can participate in hydrogen bond formation with the peptide. Aromatic rings can also be involved in hydrophobic interactions with the peptide.

We also applied a reflection ellipsometry method to determine the average film thickness on the top of the substrate and optical constants.[69,70,71] Ellipsometry measures the changes in the state of polarization of light upon reflection from the surface.[72] These changes are directly related to thickness and the refractive index n.[73,74] The film thickness is determined according to the interference between light reflecting from the surface and light traveling through the film.[75] The relevant material properties are described using the refractive index n. If the refractive indexes of the film and the substrate are known, the thickness d of the thin film can be calculated using this method.

Table 2. Results of the ellipsometric measurements.

Layer	Refractive index, n at $\lambda = 632.8$ [nm]	Thickness d [nm]
Cysteamine	1.490	1.42
Collagen-like peptide	1.194	9.22
Curcumin	1.156	0.76
Rutin	1.521	1.90
Quercetin	1.444	1.89
Naringin	1.213	2.48
Hypericin	1.510	5.69

Ellipsometry was used to measure the average thickness of the consecutive layers immobilized on a Au surface. The modifications of disks for ellipsometric measurements were performed as described in Scheme 1. The determination of the adsorbed layers' thickness was performed by fitting the experimental Ψ and Δ data using a linear regression procedure. From this fitting procedure, refractive indexes (n) were calculated, and a thickness of the consecutive layers was valuated. The thickness and refractive indexes calculated from these experiments are given in Table 2. The thicknesses of additional layers are 1.42 nm (cysteamine) and 9.22 nm (collagen-like peptide[13]). These values correspond with the monolayers. The values of the layer's thicknesses of the polyphenols presented in this paper are also in agreement with values for the monolayers formed by the polyphenols.

Absorption spectra were measured for naringin, quercitin and rutin and their mixture with the collagen-like peptide (Fig. 6). Due to

a very low solubility, as well as much lower sensitivity comparing to SPR, and any measurements were not effective for curcumin and hypericin. For naringin and the mixture, position of the absorption peaks is the same (Fig. 6a). In the light of SPR and AFM results, the possible explanation is that only sugar moiety is involved in the interactions with the peptide. For the quercitin/collagen-like peptide, the peak from the UV range is shifted towards the longer wavelength (Fig. 6b). Additionally, a blueshift and magnification of the peak from the visible light range is observed. A redshift is observed for the second most intensive peak for rutin/collagen-like peptide solution (Fig. 6c). The results indicate that for quercitin and rutin, the aromatic moiety is involved in the interaction with the collagen-like peptide.
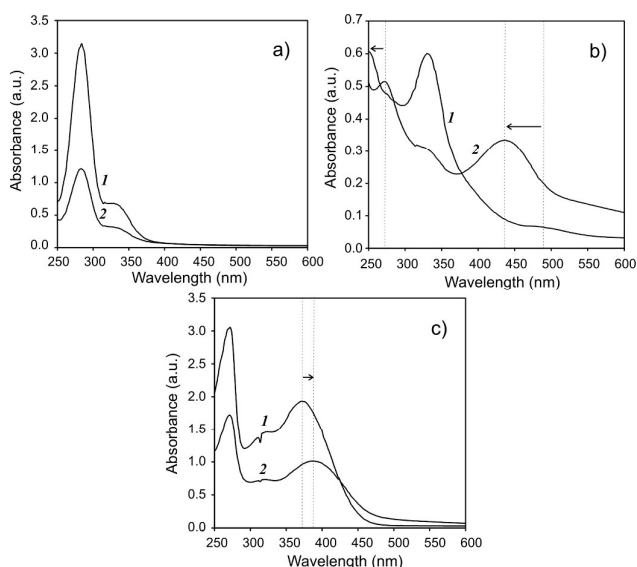

Fig. 6. UV-VIS spectra of (1) pristine polyphenols: (a) naringin, (b) quercetin and (c) rutin; and (2) their mixture with the collagen-like peptide.

Simulations

The results of the SPR and AFM experiments refer to the state in which peptides interact with the polyphenolic molecules. Due to the large number of atoms in the considered systems, we did not build a model in which the triple helical collagen-like peptide interacts with layers of polyphenolic molecules and restricted our theoretical investigations to the molecular mechanics approach. However, our molecular docking simulations provide additional complementary information that is not accessible using the SPR and AFM methods. In this study, we analyzed the preferred orientation of one selected polyphenol molecule (curcumin, rutin, quercetin, naringin, or hypericin) with the collagen-like peptide molecule when bound to each other. Many stable complexes were considered. Those with the highest binding affinity were selected and their structural parameters were shown.
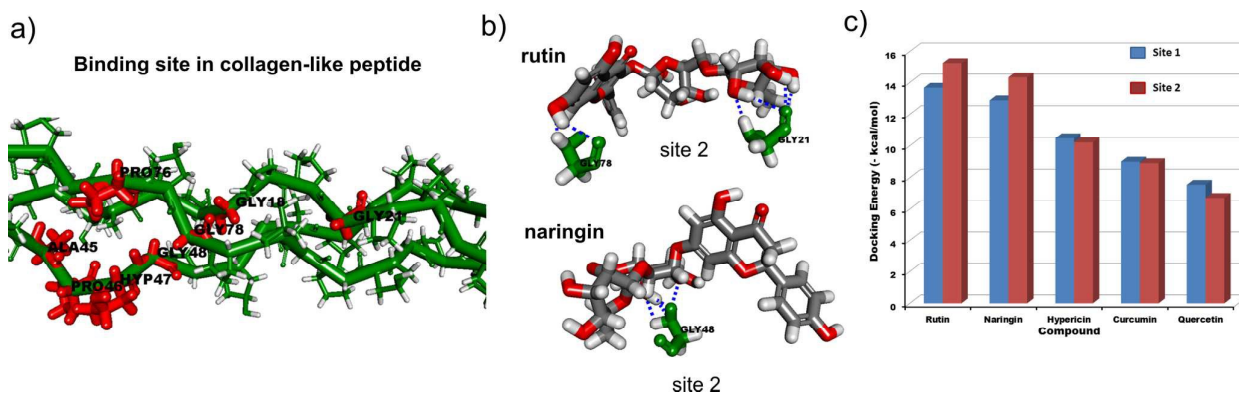
Journal Name

ARTICLE

Fig. 7. (a) The overall putative binding site residues of collagen. (b) Site 2 (lowest docking energy site) binding site residues of collagen making hydrogen bonds with rutin and naringin. (c) Docking energy of the polyphenols with the collagen-like peptides.

The binding analysis of all five polyphenolic compounds (**1-5**) on the collagen structure revealed that these molecules bind at the predicted active site residues of Gly 18, Gly 21, Ala 45, Pro 46, Hyp 47, Gly 48, Pro 76 and Gly 78 on collagen-like peptides by making hydrogen bond interactions (Fig. 7a). The docking simulations predicted that rutin plant metabolite has a higher affinity for collagen compared with other compounds (Fig. 7b). Site 2 on the structure of collagen produced the lowest docking energy (DE: -15.26 kcal mol^{-1}) compared with site 1 (DE: -13.67 kcal mol^{-1}) (Fig. 7b). Naringin also shared close affinity with collagen, which is determined by docking energy. In this scenario, site 2 also showed higher affinity for naringin with a docking energy of -14.33 kcal mol^{-1} compared with site 1 (which had a docking energy of -12.88 kcal mol^{-1}). A binding site residue analysis revealed that rutin makes hydrogen bonds with Gly 21 and Gly 78 amino acid residues and that naringin makes a hydrogen bond with the Gly 48 residue (Fig. 7b).

The theoretically predicted docking energies (the sum of the intermolecular and internal energy) indicate the strength of the association between collagen-like peptide and polyphenolic molecules. Our results add to the body of experimental studies of the collagen-like peptide and polyphenolic compounds interactions, particularly the analysis of structural changes upon the complex formation. We directly label the intermolecular hydrogen bonds involved with the interaction of the collagen-like peptide with polyphenolic molecules. However, the obtained docking energies and the respective order of the polyphenolic compounds (Fig. 7c) cannot be directly compared with the results of the SPR experiment. The molecular modelling studies of the intramolecular interactions between layers of polyphenolic compounds and their binding affinities with collagen-like peptide call for separate extensive studies and involve a new parameterisation of the force-field in the

molecular mechanics approach.

Conclusions

Understanding the interactions between collagen and polyphenols could provide important insight into the potential use of particular polyphenolic compounds as stabilizing agents. The layer-by-layer assembly process on a Au surface by collagen and polyphenols was traced via SPR and AFM. Both methods revealed the following order of affinity for collagen: hypericin>naringin>quercetin>curcumin>rutin. The differences in the binding patterns can be attributed to the structural differences of polyphenols.

Experimental

Materials and Methods

The following chemicals were used as received without further purification: Tris-buffered saline (pH 8.0, solution in 1 L deionized water: 0.05 M Tris, 0.138 M NaCl, 0.0027 M HCl), cysteamine (2-mercaptoethylamine) (~95%, Sigma Aldrich), 1-(3-dimethylaminopropyl)-3-ethylcarbodiimide hydrochloride (EDC, ≥98%, Alfa Aesar), *N*-hydroxysuccinimide (NHS, ≥97%, Fluka), anhydrous ethanol (99,8%, POCH), naringin (naringenin 7-O-β-D-(-2″-α-L-rhamnosyl)-glucoside from citrus fruit (≥90%, Sigma Aldrich)), curcumin (diferuloylmethane) from *Curcuma longa* (Turmeric) (≥60%, Sigma Aldrich) and hypericin (HWI Analytik GmbH). Quercetin (3,3′,4′,5,6-pentahydroxyflavone) and rutin (quercetin 3-O-β-D-(-6″-α-L-rhamnosyl)-glucoside) were isolated as described previously.[76] Both substances had a purity

of ≥95%. The thirty-amino acid collagen-like peptide was acquired from LifeTein LLC. (cat. No. 293324; sequence: (Pro-Hyp-Gly)$_4$-Pro-Hyp-Ala-(Pro-Hyp-Gly)$_5$). All aqueous solutions were prepared using deionized water, which was further purified with a Milli-Q system.

AFM was performed using 5500 AFM (Agilent Technologies, currently Keysight Technologies, Santa Clara, CA, USA). All data were recorded under ambient conditions in air. The values of the initial current were always sufficiently high to provide contact between the tip and the molecules adsorbed on the Au surface. AFM images were obtained in tapping mode in a computer-controlled modular system using PicoView 1.12 and Pico Image Basic software.

SPR measurements were obtained with an AutoLab SPRINGLE SPR system with hardware and software from Eco Chemie B.V. (The Netherlands). Surface plasmon spectroscopic data were collected using Kretschmann optical configuration. The SPR spectrometer was equipped with a GaAs laser diode, which was fixed at the wavelength of 670 nm using a vibrating mirror to modulate the angle of incidence of the p-polarized light beam on the SPR substrate. The SPR sensor disk with Au coating on a glass surface with a 25-mm diameter. An O-ring (inner diameter 4 mm) between the cuvette and the disk prevented leakage. The gold disk was placed inside the equipment on the base of a hemicylindrical lens (ZK7, n=1.61) with index-matching oil to establish an optical entity (n=1.61). All SPR measurements were conducted at 20.5°C. The measured Dq values correspond to the amount of adsorbed material with a mass sensitivity factor of 120 mdeg per 100 ng cm^{-2}.

Ellipsometric measurements were made with a SENTECH Instruments GmbH SE850 manual thin-film ellipsometer using a HeNe laser (632.8 nm) at an angle of incidence of 70 ± 0.02°. The light spot was 1 x 3 mm^2. The measurements were performed in the spectral range from 250 to 850 nm with sampling steps of 5 nm. The changes in the state of polarization of light upon reflection on the sample surface were accounted for using the ellipsometric parameters Ψ and Δ. Ψ is related to the change of intensity between the incident and reflected beams. Δ accounts for the phase shift. These ellipsometric angles are related to the refractive index *n* and thickness *d* of the film. The ellipsometric data were fitted using the commercial software SpectraRAY 3 from SENTECH Instruments GmbH.

Absorption spectroscopy study

5.0 mg of the peptide was dissolved in 5% acetic acid to a final concentration of 100 mg·mL^{-1} and was incubated overnight at 277 K. Then, the solution was mixed with an equal volume of 1M Tris base. 20 µL of the peptide solution or pristine acetate/Tris buffer was mixed with 80 µL of polyphenols suspended in the same buffer as the peptide, incubated for two hours at 277 K and centrifuged. Next, 100 µL of the supernatant was transferred to 96-well microplate UV-VIS spectra were measured at 25°C on microplate reader (Tecan Infinite M200 Pro) with the acetate/Tris buffer as a blank.

Crystallographic study

Crystallization and crystal handling

Crystallization of collagen-like peptide was carried out as previously described.[13] Briefly, the peptide was dissolved in 10% acetic acid to a final concentration of 20.0 mg·mL^{-1} and was incubated overnight at 277 K. Then, the solution was mixed with an equal volume of 40%

PEG 400 and used for crystallization. Crystals were grown using the hanging drop vapour diffusion method at 277 K by equilibrating the 5 µL of the peptide solution against 1.0 mL of the 20% PEG 400. The crystals appeared within a week. Prior to soaking with polyphenolic compounds, the crystals were washed and transferred to 3 µL drops of Tris-buffered saline pH 8.0 (2.7 mM KCl, 138 mM NaCl and 50 mM TrisHCl) supplemented with 20% PEG 400. After overnight incubation, 3 µL of the ligands' suspension (curcumin, rutin, quercetin and naringin) in the same solution was added. Due to the very low solubility of hypericin in aqueous solution, this ligand was omitted for crystallographic study. The crystals were soaked for one month.

Table 3. Crystallographic data and refinement statistics. Values in parentheses are for the last resolution shell.

Data collection and processing statistics	
Data set	Collagen-like peptide
Beamline	BESSY BL14.2
Wavelength (Å)	0.91841
Temperature (K)	100
Space group	*C*2
Cell dimensions (Å, °)	
a	171.6
b	13.9
c	25.0
β	94.6
Mosaicity (°)	0.20
Resolution range (Å)	28.5-1.27 (1.35-1.27) [a]
Total reflections	60616
Unique reflections	16057
Completeness (%)	99.6 (93.7)
Multiplicity	3.8 (3.0)
<I/σ(I)>	17.1 (8.0)
R_{merge} [b]	0.052 (0.148)
Refinement statistics	
Resolution (Å)	28.50-1.27
No. of reflections in working / test set	15012 / 1044
R / R_{free} [c]	0.137/0.171
No. of atoms (protein/water)	497/188
R.m.s. deviation from ideal	
bond lengths (Å)	0.013
bond angles (°)	2.03
Average B factor (Å^2)	8.2
Ramachandran statistics (%) favoured	
most favoured regions	100
PDB code	4Z1R

[a] The values in parentheses correspond to the last resolution shell. [b] R_{merge} = $\Sigma_{hkl}\Sigma_i|I_i$ (hkl) − <I(hkl)>|/$\Sigma_{hkl}\Sigma_iI_i$(hkl), where <I(hkl)> is the average intensity of reflection hkl. [c] R = $\Sigma_{hkl}||F_o(hkl)|$ − |F_c(hkl)|| / $\Sigma_{hkl}|F_o$(hkl)|, where F_o and F_c are the observed and calculated structure factors, respectively. R_{free} is calculated analogously for the test reflections, which were randomly selected and excluded from the refinement.

Data collection and processing

The crystals were transferred to a cryoprotectant solution containing the Tris-buffered saline pH 8.0 and 33% PEG 400 supplemented with adequate polyphenolic compound at a saturation concentration and vitrified in liquid nitrogen. X-ray diffraction data were measured at the BESSY synchrotron (Berlin, Germany) beamline BL14.2 to a resolution of up to 1.27 Å (crystal soaked with quercetin). The crystals are monoclinic and belong to the space group *C2*. All diffraction images were processed and scaled with *XDS*.[77] Data collection and processing statistics are presented in Table 3.

ARTICLE

Structure determination and refinement

The structure was solved and refined based on diffraction data collected for the crystal soaked with quercetin. The collagen-like peptide crystal is isomorphous with the previously described crystal structure (PDB code 1CAG).[13] The PDB model 1CAG, which was stripped of all water molecules and acetate ions, was placed in the nearly identical unit cell of the crystal. Anisotropic stereochemically restrained structure-factor refinement was performed in *REFMAC5* using maximum likelihood targets. Due to the absence of electron density, four disordered regions corresponding to residues 28-30 (chain A), 1-2 and 29-30 (chain B), and 1-2 and 28-30 (chain C) could not be modelled and were not included in the refinement. Additionally, 188 water molecules were included in the final set of atomic coordinates. The rounds of *REFMAC5* refinement were interspersed with manual model rebuilding in *COOT*.[78] The stereochemical quality of the models was assessed with the wwPDB validation server.[79] The final refinement statistics for the collagen-like peptide are reported in Table 1. The atomic coordinates and structure factors have been deposited in the RCSB Protein Data Bank with the accession code 4Z1R.

Molecular docking of plants metabolites with collagen

SMILES strings of polyphenols were obtained from the PUBCHEM database and furnished to the CORINA server to obtain their 3D structures. All 3D structure files were saved in the pdb file format (http://www.molecular -networks.com/online_demos/corina_demo). The molecular docking of these compounds was performed against collagen peptide (pdb id: 1CAG) using the Autodock.v.4.2 software. The complete docking process was divided into three steps: (i) addition of the missing atoms in the structure of the collagen peptide; (ii) preparation of tripeptide and flavonoid structures prior to the final docking process, such as the addition of hydrogens and all atomic charges, etc.; (iii) docking simulation of compounds against collagen peptide structure. Note that the collagen peptide structure is straight and difficult to accommodate into the maximum grid box dimensions of the Autogrid process, i.e., x=126, y=126 and z=126. Therefore, the docking process was separately performed on the two halves of the tripeptide structure, i.e., the grid box was generated on the two halves of the collagen peptide structure, and the docking simulations were performed independently.

Prior to the docking process, the structure of the collagen peptide was checked using Swiss-PdbViewer software for the addition of the missing atoms. The output file was saved in PDB format. Furthermore, the structures of the collagen peptide and the flavonoids were prepared prior to the final docking simulations via Autodock.v.4.2 software. All hydrogen atoms were added on both the structures of the collagen peptide and the flavonoids via AutoDockTools. The Gasteiger and Kollman United Atom charges were assigned to the polyphenols and collagen peptide, respectively. The maximum number of the rotatable bonds was selected for these molecules to provide the maximum degree of freedom to their bonds. Furthermore, the Grid box was separately generated around the two halves (left and right) of the collagen peptide structure with the grid point dimensions of x=126, y=80 and z=98 as well as grid point spacing of 0.375 Å. Note that the overall structure of the two parts of the collagen peptide was taken as the docking target. The docking simulation was performed using the Genetic Algorithm-Local Search (GA-LS) algorithm with the following parameters: the

number of translation step was set to 0.02 per Å, the number of individuals in the population (ga population size) was maintained at 150, the maximum number of energy evaluations (ga_num_evals, 2500000) and maximum number of generations (ga_num_generations, 27000) were performed to obtain good accuracy, the rate of gene mutation (ga_mutation_rate, 0.02) was set to a smaller value to obtain complete coverage of the docking process and the rate of crossover (ga_crossover_rate) was set to 0.8. The complete docking simulation was performed for 200 GA cycles. Different conformations of the compounds obtained after the docking process were clustered based on their binding energies with a root-mean-square deviation tolerance of 2.0 Å, and their respective docking energies were calculated. The best conformations of the natural plant metabolites were selected based on their lowest docking energies (the sum of the intermolecular and internal energy) on the structure of the collagen peptide.

References

1   V. A. Kumar, N. L. Taylor, A. A. Jalan, L. K. Hwang, B. K. Wang and J. D. Hartgerink, *Biomacromolecules*, 2014, **15**, 1484–1490.
2   J. Ward, J. Kelly, W. Wang, D. I. Zeugolis and A. Pandit, *Biomacromolecules*, 2010, **11**, 3093–3101.
3   K. von der Mark, *Int. Rev. Connect. Tissue Res.*, 1981, **9**, 265–324.
4   W. H. C. Tiong, G. Damodaran, H. Naik, J. L. Kelly and A. Pandit, *Langmuir*, 2008, **24**, 11752–11761.
5   J. D'Armiento, *J. Clin. Invest.*, 2003, **112**, 1308–1310.
6   G. Faury, M. Pezet, R. H. Knutsen, W. A. Boyle, S. P. Heximer, S. E. McLean, R. K. Minkes, K. J. Blumer, A. Kovacs, D. P. Kelly, D. Y. Li, B. Starcher and R. P. Mecham, *J. Clin. Invest.*, 2003, **112**, 1419–1428.
7   L. Cen, W. Liu, L. Cui, W. Zhang and Y. Cao, *Pediatr. Res.*, 2008, **63**, 492–496.
8   D. L. Ellis and I. V. Yannas, *Biomaterials*, 1996, **17**, 291–299.
9   R. Marchand, S. Woerly, L. Bertrand and N. Valdes, *Brain Res. Bull.*, 1993, **30**, 415–422.
10 A. Mandal, S. Panigrahi and C. Zhang, *Biol. Eng.*, 2010, **2**, 63–88.
11 H. Hofmann, P. P. Fietzek and K. Kühn, *J. Mol. Biol.*, 1978, **125**, 137–165.
12 R. S. Erdmann and H. Wennemers, *Angew. Chem. Int. Ed.*, 2011, **50**, 6835–6838.
13 J. Bella, M. Eaton, B. Brodsky and H. M. Berman, *Science*, 1994, **266**, 75–81.
14 R. D. B. Fraser, T. P. MacRae and E. Suzuki, *J. Mol. Biol.*, 1979, **129**, 463–481.
15 B. Madhan, C. Muralidharan and R. Jayakumar, *Biomaterials*, 2002, **23**, 2841–2847.
16 N. Vyavahare, M. Ogle, F. J. Schoen and R. J. Levy, *Am. J. Pathol.*, 1999, **155**, 973–982.

17 M. Bailey, H. Xiao, M. Ogle and N. Vyavahare, *Am. J. Pathol.*, 2001, **159**, 1981–1986.

18 S. K. Wasser, S. L. Monfort and D. E. Wildt, *J. Reprod. Fertil.*, 1991, **92**, 415–423.

19 D. P. Speer, E. E. Peacock and M. Chvapil, *J. Surg. Res.*, 1975, **19**, 169–173.

20 J. Mlczoch, W. Zutter, R. Keller and H. Herzog, *Respir. Int. Rev. Thorac. Dis.*, 1975, **32**, 424–435.

21 R. Swamy, A. Gnanamani, S. Shanmugasamy, R. Gopal and A. Mandal, *BMC Res. Notes*, 2011, **4**, 399.

22 D. I. Zeugolis, P. P. Panengad, E. S. Y. Yew, C. Sheppard, T. T. Phan and M. Raghunath, *J. Biomed. Mater. Res. A*, 2009, **9999A**, NA–NA.

23 G. Damodaran, R. Collighan, M. Griffin and A. Pandit, *J. Biomed. Mater. Res. A*, 2009, **89A**, 1001–1010.

24 L. H. H. Olde Damink, P. J. Dijkstra, M. J. A. Van Luyn, P. B. Van Wachem, P. Nieuwenhuis and J. Feijen, *J. Mater. Sci. Mater. Med.*, 1995, **6**, 460–472.

25 J. E. Gough, C. A. Scotchford and S. Downes, *J. Biomed. Mater. Res.*, 2002, **61**, 121–130.

26 H. G. Sundararaghavan, G. A. Monteiro, N. A. Lapin, Y. J. Chabal, J. R. Miksan and D. I. Shreiber, *J. Biomed. Mater. Res. A*, 2008, **87A**, 308–320.

27 L.-P. Yan, Y.-J. Wang, L. Ren, G. Wu, S. G. Caridade, J.-B. Fan, L.-Y. Wang, P.-H. Ji, J. M. Oliveira, J. T. Oliveira, J. F. Mano and R. L. Reis, *J. Biomed. Mater. Res. A*, 2010, **95A**, 465–475.

28 B. Hafemann, K. Ghofrani, H. G. Gattner, H. Stieve and N. Pallua, *J. Mater. Sci. Mater. Med.*, 2001, **12**, 437–446.

29 M. L. Jarman-Smith, T. Bodamyali, C. Stevens, J. A. Howell, M. Horrocks and J. B. Chaudhuri, *J. Mater. Sci. Mater. Med.*, 2004, **15**, 925–932.

30 B. Madhan, V. Subramanian, J. R. Rao, B. U. Nair and T. Ramasami, *Int. J. Biol. Macromol.*, 2005, **37**, 47–53.

31 J. C. Isenburg, D. T. Simionescu and N. R. Vyavahare, *Biomaterials*, 2005, **26**, 1237–1245.

32 J. C. Isenburg, N. V. Karamchandani, D. T. Simionescu and N. R. Vyavahare, *Biomaterials*, 2006, **27**, 3645–3651.

33 H. R. Tang, A. D. Covington and R. A. Hancock, *Biopolymers*, 2003, **70**, 403–413.

34 H. R. Tang, A. D. Covington and R. A. Hancock, *J. Agric. Food Chem.*, 2003, **51**, 6652–6656.

35 J. A. Vita, *Am. J. Clin. Nutr.*, 2005, **81**, 292S–297S.

36 H. Yamada and H. Watanabe, *Cardiovasc. Res.*, 2007, **73**, 439–440.

37 M. Quiñones, M. Miguel and A. Aleixandre, *Pharmacol. Res.*, 2013, **68**, 125–131.

38 R. Tsao, *Nutrients*, 2010, **2**, 1231–1246.

39 K. B. Pandey and S. I. Rizvi, *Oxid. Med. Cell. Longev.*, 2009, **2**, 270–278.

40 Y. Kuroda and Y. Hara, *Mutat. Res.*, 1999, **436**, 69–97.

41 C. S. Yang, J. D. Lambert and S. Sang, *Arch. Toxicol.*, 2009, **83**, 11–21.

42 N. Venkatesan, D. Punithavathi and V. Arumugam, *Br. J. Pharmacol.*, 2000, **129**, 231–234.

43 P. S. Babu and K. Srinivasan, *Mol. Cell. Biochem.*, 1995, **152**, 13–21.

44 B. Rathi, *Sci. Pharm.*, 2013, **81**, 567–589.

45 S. Saravanan, K. Arunachalam and T. Parimelazhagan, *Ind. Crops Prod.*, 2014, **54**, 272–280.

46 J. Davila, D. Toulemon, T. Garnier, A. Garnier, B. Senger, J.-C. Voegel, P. J. Mésini, P. Schaaf, F. Boulmedais and L. Jierry, *Langmuir*, 2013, **29**, 7488–7498.

47 A. W. Wark, H. J. Lee and R. M. Corn, *Anal. Chem.*, 2005, **77**, 3904–3907.

48 M. Shalev and A. Miriam, *Materials*, 2011, **4**, 469–486.

49 D. Avnir, S. Braun, O. Lev and M. Ottolenghi, *Chem. Mater.*, 1994, **6**, 1605–1614.

50 C. Aicart-Ramos, M. Valhondo Falcón, P. R. Ortiz de Montellano and I. Rodriguez-Crespo, *Biochemistry (Mosc.)*, 2012, **51**, 7403–7416.

51 S. Choi and J. Chae, *J. Assoc. Lab. Autom.*, 2010, **15**, 172–178.

52 R. Bakhtiar, *J. Chem. Educ.*, 2013, **90**, 203–209.

53 S. Vutukuru, S. R. Bethi and R. S. Kane, *Langmuir*, 2006, **22**, 10152–10156.

54 R. Georgiadis, K. P. Peterlinz and A. W. Peterson, *J. Am. Chem. Soc.*, 2000, **122**, 3166–3173.

55 Y. Yanase, T. Hiragun, S. Kaneko, H. J. Gould, M. W. Greaves and M. Hide, *Biosens. Bioelectron.*, 2010, **26**, 674–681.

56 J. M. Luther, P. K. Jain, T. Ewers and A. P. Alivisatos, *Nat. Mater.*, 2011, **10**, 361–366.

57 D. J. Taatjes, A. S. Quinn, J. H. Rand and B. P. Jena, *J. Cell. Physiol.*, 2013, **228**, 1949–1955.

58 L. Gross, F. Mohn, N. Moll, P. Liljeroth and G. Meyer, *Science*, 2009, **325**, 1110–1114.

59 L. Newton, T. Slater, N. Clark and A. Vijayaraghavan, *J Mater Chem C*, 2013, **1**, 376–393.

60 K. Kpegba, T. Spadaro, R. B. Cody, N. Nesnas and J. A. Olson, *Anal. Chem.*, 2007, **79**, 5479–5483.

61 R. Z. Kramer, L. Vitagliano, J. Bella, R. Berisio, L. Mazzarella, B. Brodsky, A. Zagari and H. M. Berman, *J. Mol. Biol.*, 1998, **280**, 623–638.

62 J. Bella, J. Liu, R. Kramer, B. Brodsky and H. M. Berman, *J. Mol. Biol.*, 2006, **362**, 298–311.

63 C. G. Long, M. H. Li, J. Baum and B. Brodsky, *J. Mol. Biol.*, 1992, **225**, 1–4.

64 C. G. Long, E. Braswell, D. Zhu, J. Apigo, J. Baum and B. Brodsky, *Biochemistry (Mosc.)*, 1993, **32**, 11688–11695.

65 J. C. Rodríguez Hernández, M. Salmerón Sánchez, J. M. Soria, J. L. Gómez Ribelles and M. Monleón Pradas, *Biophys. J.*, 2007, **93**, 202–207.

66 D. P. Allison, P. Hinterdorfer and W. Han, *Curr. Opin. Biotechnol.*, 2002, **13**, 47–51.

67 E. Peli, *J. Opt. Soc. Am. A*, 1990, **7**, 2032.

68 J. Borch and P. Roepstorff, *Anal. Chem.*, 2004, **76**, 5243–5248.

69 W. Wang, C. Qi, T. Kang, Y. Niu, G. Jin, Y. Ge and Y. Chen, *Anal. Chem.*, 2013, **85**, 4446–4452.

70 A. García-Marín, J. M. Abad, E. Ruiz, E. Lorenzo, J. Piqueras and J. L. Pau, *Anal. Chem.*, 2014, **86**, 4969–4976.

71 F. Höök, B. Kasemo, T. Nylander, C. Fant, K. Sott and H. Elwing, *Anal. Chem.*, 2001, **73**, 5796–5804.

72 G. B. Sigal, C. Bamdad, A. Barberis, J. Strominger and G. M. Whitesides, *Anal. Chem.*, 1996, **68**, 490–497.

73 M. G. Muñoz, F. Monroy, F. Ortega, R. G. Rubio and D. Langevin, *Langmuir*, 2000, **16**, 1083–1093.

74 Y. M. Bae, B.-K. Oh, W. Lee, W. H. Lee and J.-W. Choi, *Anal. Chem.*, 2004, **76**, 1799–1803.

75 Y.-J. Li, Y. Zhang and F. Zhou, *Anal. Chem.*, 2008, **80**, 891–897.

76 M. Tomczyk, *Biochem. Syst. Ecol.*, 2006, **34**, 770–773.

77 W. Kabsch, *Acta Crystallogr. D Biol. Crystallogr.*, 2010, **66**, 125–132.

78 P. Emsley, B. Lohkamp, W. G. Scott and K. Cowtan, *Acta Crystallogr. D Biol. Crystallogr.*, 2010, **66**, 486–501.

79 H. Berman, K. Henrick and H. Nakamura, *Nat. Struct. Biol.*, 2003, **10**, 980–980.